Supplemental Materials

Piezo1-mediated mechanosensation in bone marrow macrophages promotes vascular niche regeneration after irradiation injury

Xiaomei Zhang[1], Lijia Hou[1], Fengjie Li[1], Weiwei Zhang[1], Chun Wu[1], Lixin Xiang[1], Jiuxuan Li[1], Luping Zhou[1], Xiaojie Wang[1], Yang Xiang[1], Yanni Xiao[2], Shengwen Calvin Li[3,4], Li Chen[1*], Qian Ran[1*], Zhongjun Li[1*]

[1] Laboratory of Radiation Biology, Laboratory Medicine Center, Department of Blood Transfusion, The Second Affiliated Hospital, Army Military Medical University, Chongqing 400037, China

[2] 111 Project Laboratory of Biomechanics and Tissue Repair, College of Bioengineering, Chongqing University, Chongqing 400044, China

[3] CHOC Children's Research Institute, Children's Hospital of Orange County (CHOC); Orange, CA 92868, USA

[4] Department of Neurology, University of California-Irvine School of Medicine, Orange, CA 92868, USA

[*]**Correspondence**: iceman@tmmu.edu.cn; louise-r-q@tmmu.edu.cn; shengwel@uci.edu; zhongjunli@tmmu.edu.cn.

Laboratory of Radiation Biology, Laboratory Medicine Center, Department of Blood Transfusion, The Second Affiliated Hospital, Army Military Medical University, Xinqiao Road, Shapingba, Chongqing 400037, China

Supplemental Figures and Legends

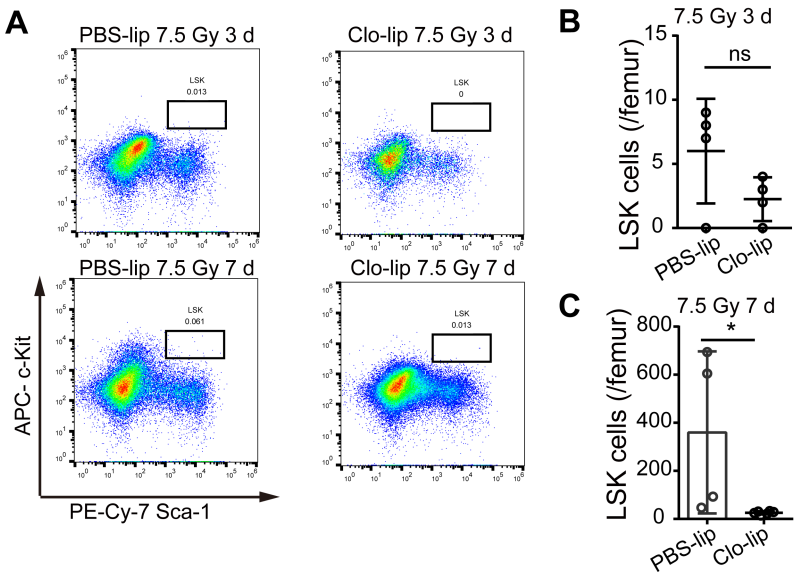

Figure S1. Depletion of residual BM-Mφ impedes LSKs regeneration after 7.5 Gy irradiation. (A) Representative flow cytometry analysis of LSKs in the femur after 7.5 Gy irradiation with PBS-lip or Clo-lip injection. **(B-C)** Number of LSKs per femur at 3 days **(B)** and 7 days **(C)** after 7.5 Gy irradiation with PBS-lip or Clo-lip injection (n = 4 mice, *t*-test). * $P < 0.05$; ns, not significant.

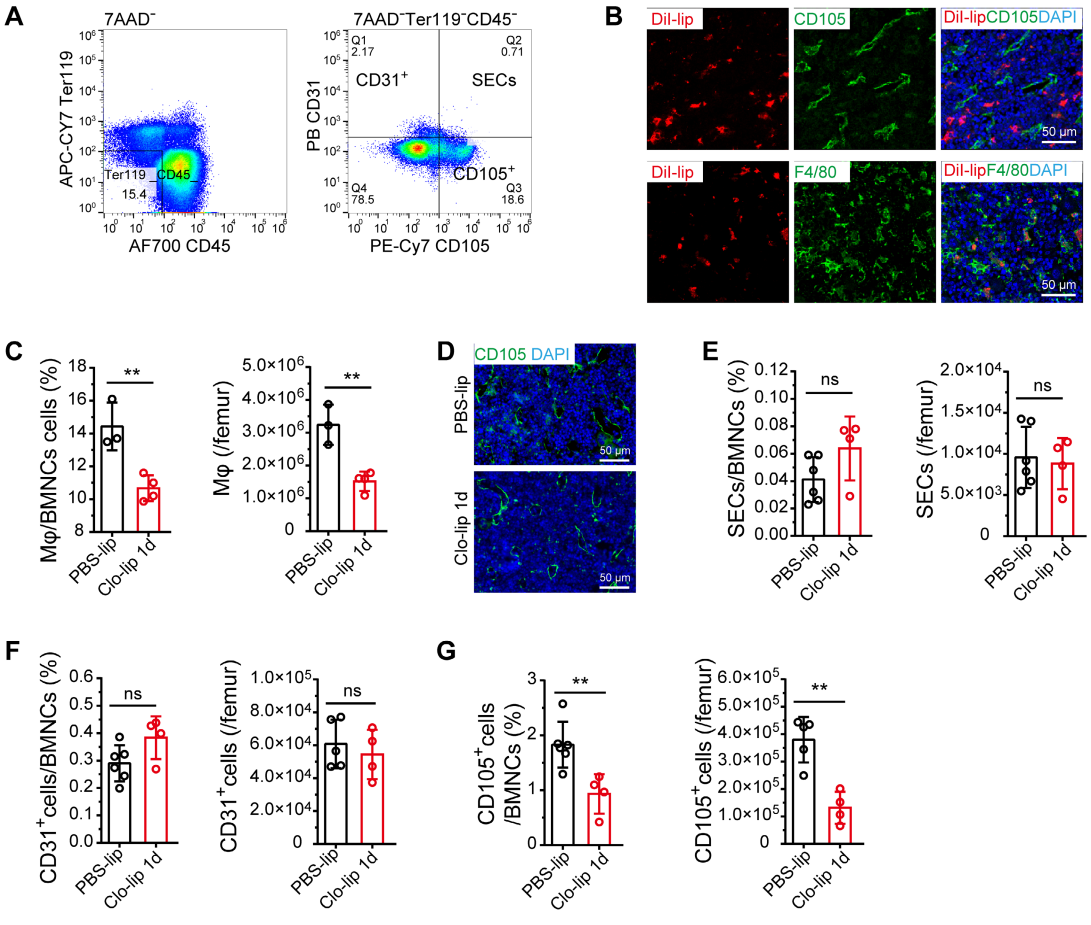

Figure S2. Effect of BM-Mφ depletion by Clo-lip on sinusoids at steady state. (A) Representative flow cytometry analysis of bone marrow sinusoidal endothelial cells (SECs). **(B)** *In situ* immunofluorescence images showing bone marrow cells that have engulfed DiI-labeling liposomes (DiI-lip) (red), bone marrow sinusoids (green, CD105), and BM-Mφ (green, F4/80). The nucleus was stained with DAPI (blue). Scale bar, 50 μm. **(C)** Frequency of BM-Mφ in BMNCs and number of BM-Mφ per femur. **(D)** *In situ* immunofluorescence images showing bone marrow sinusoids (green, CD105) after 1 day with Clo-lip or PBS-lip treatment under non-irradiation conditions. **(E)** Frequency of SECs in BMNCs and number of SECs per femur, **(F)** frequency of $CD31^+$ECs in BMNCs and number of $CD31^+$ECs per femur, **(G)** frequency of $CD105^+$ stromal cells in BMNCs, and the number of $CD105^+$ stromal cells per femur analyzed by flow cytometry at 1 day after Clo-lip or PBS-lip injection (n = 4–6 mice, *t*-test). Data were shown as mean ± SD. $^{**}P < 0.01$; ns, not significant.

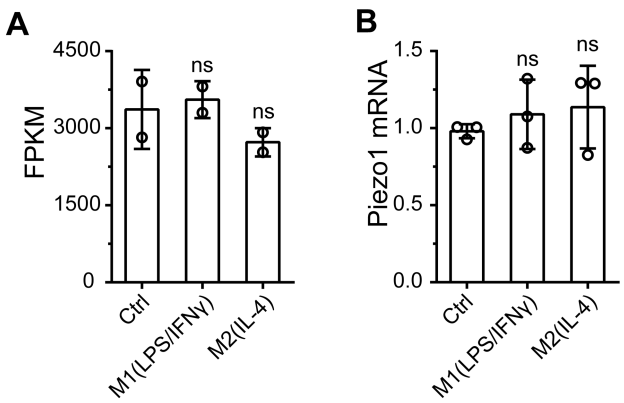

Figure S3. Piezo1 expression in classical M1 and M2 activation in BMDMs. BMDMs were treated with 50 ng/mL LPS and 20 ng/mL IFNγ or 100 ng/mL IL-4 for 6 h *in vitro*. **(A)** FPKM of Prizo1 in non-activated BMDMs (Ctrl), M1 and M2 BMDMs (ref: GES113836) (n = 2 independent experiments, Tukey test). **(B)** RT-PCR analysis of Piezo1 mRNA level in BMDMs after activation or not (n = 3 independent experiments, Tukey test). Data were shown as mean ± SD. ns, not significant.

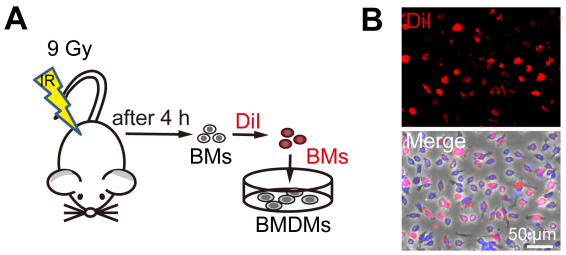

Figure. S4 Phagocytosis of irradiation-induced apoptotic bone marrow cells (BMs) by BMDMs *in vitro*. (A) Diagram showing phagocytosis of irradiation-induced apoptotic BMs by BMDMs *in vitro*. **(B)** Representative immunofluorescence images showing BMDMs that have engulfed DiI-labeling irradiation-induced apoptotic BMs (red). Scale bar, 50 μm.

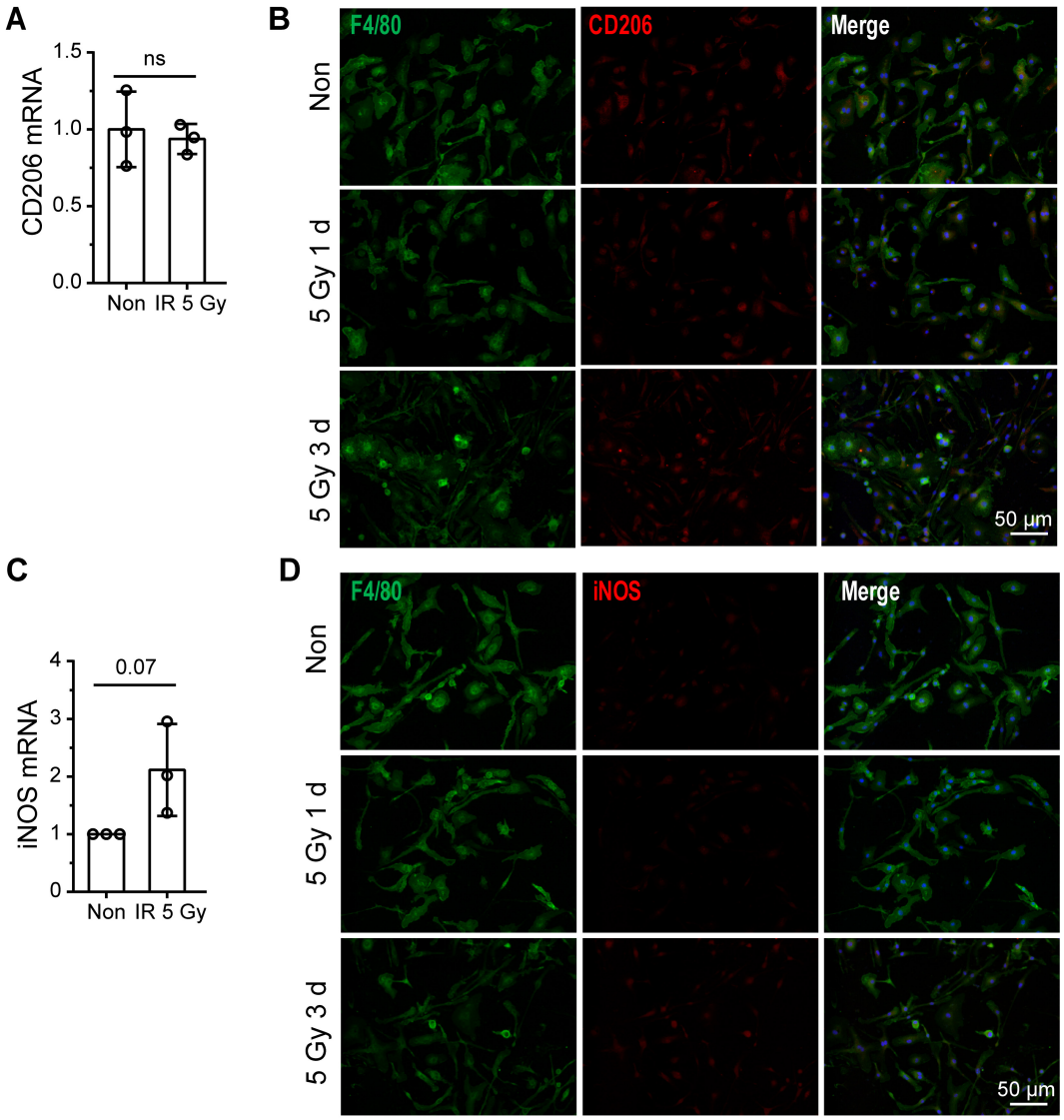

Figure. S5 Direct effects of irradiation on BMDMs activation. (A) RT-PCR analysis of CD206 (M2-type Mφ maker) mRNA levels in BMDMs 24 h after irradiation (n = 3 independent experiments, *t*-test). **(B)** Representative immunofluorescence images showing expression of CD206 in BMDMs at 24 h after irradiation. **(C)** RT-PCR analysis of iNOS (M1-type Mφ maker) in BMDMs 24 h after irradiation (n = 3 independent experiments, *t*-test). **(D)** Representative immunofluorescence images showing expression of iNOS in BMDMs at 24 h after irradiation. Scale bar, 50 μm. Data were shown as mean ± SD. ns, not significant (*t*-test).

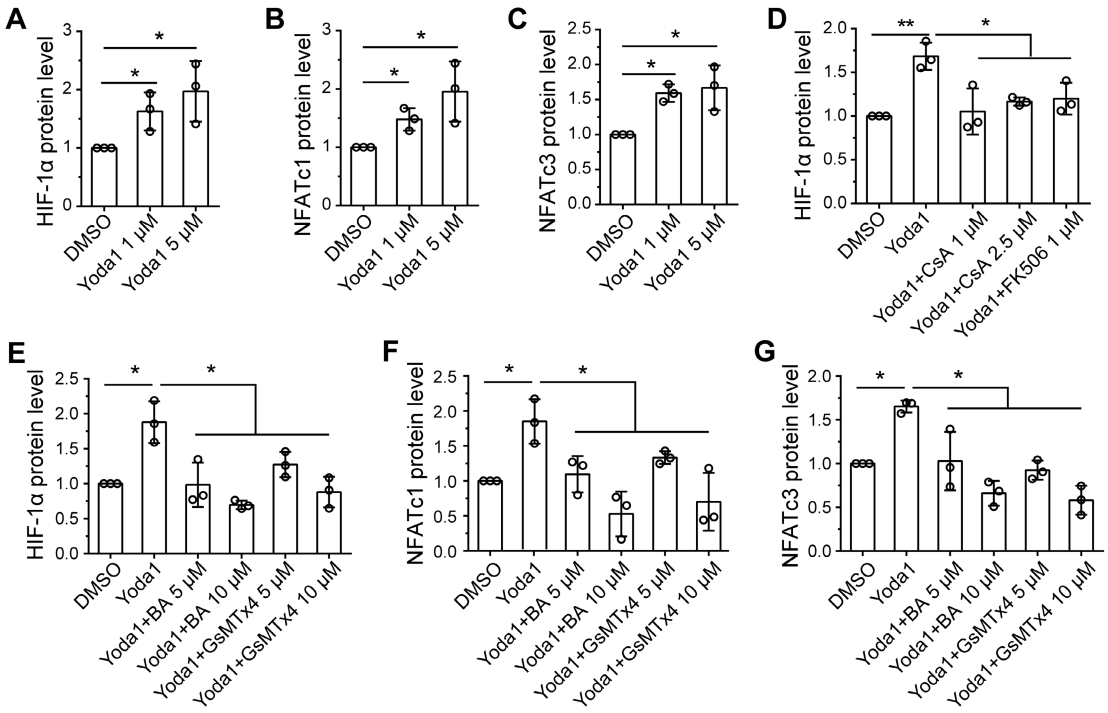

Figure S6. The quantitative analysis of the relative protein levels of Western blots in Figure 7. Protein expression was quantified by densitometry and normalized to GAPDH. **(A)** The quantitative analysis of HIF-1α protein level in Fig Figure 7B. **(B-C)** The quantitative analysis of NFATc1 and NFATc3 protein levels in Figure 7E. **(D)** The quantitative analysis of HIF-1α protein level in Figure 7F. **(E-G)** The quantitative analysis of HIF-1α, NFATc1, and NFATc3 protein levels in Figure 7I. n = 3 independent experiments, Tukey test. Data were shown as mean ± SD.*$P < 0.05$; *$P < 0.01$.

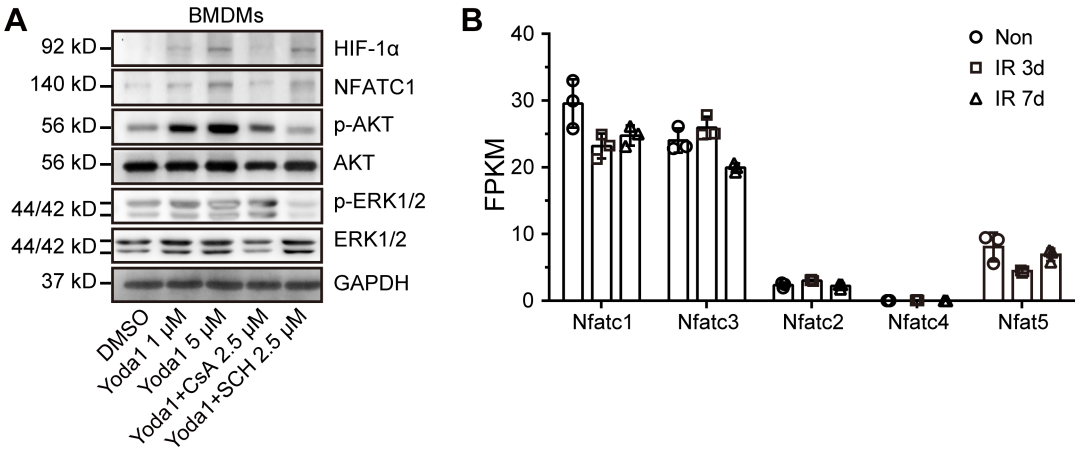

Figure. S7 The roles of ERK, AKT, and NFATs in Yoda1 induced HIF-1α accumulation. (A) Western blot analysis of HIF-1α, NFATC1, p-AKT, AKT, p-ERK1/2, ERK, and GAPDH in BMDMs pretreated with CsA or SCH for 30 min before 24 h Yoda1 (5 μM) treatment. Blots are representative of three independent experiments. **(B)** Expression analysis of NFATs in BM-Mφ from mice after 5 Gy irradiation (IR) or non-irradiation (Non) (n = 3 mice). Data were shown as mean ± SD. FPKM: fragments per kilobase million.

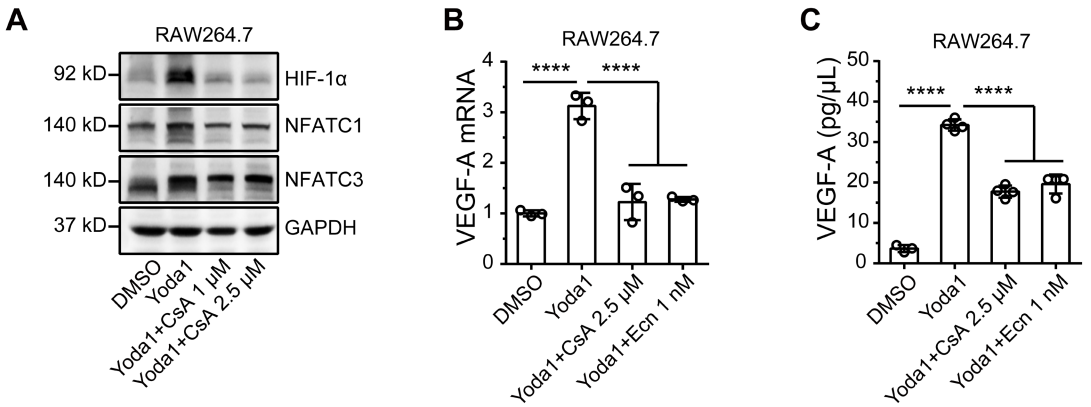

Figure S8. The activation of calcineurin/NFAT/HIF-1α signaling is responsible for Piezo1-mediated VEGF-A upexpression in RAW264.7 cells. (A) Western blot analysis of HIF-1α, NFATC1, and NFATC3 in RAW264.7 cells pretreated with CsA for 30 min before 24 h Yoda1 (5 μM) treatment. Blots are representative of three independent experiments. **(B)** RT-PCR analysis of VEGF-A mRNA levels in RAW264.7 cells pretreated with CsA or Ecn for 30 min before 6 h Yoda1 (5 μM) treatment (n = 3 independent experiments, Tukey test). **(C)** ELISA analysis of VEGF-A expression in RAW264.7 cells pretreated with CsA or Ecn for 30 min before 24 h Yoda1 (5 μM) treatment (n = 4 independent experiments, Tukey test). Data were shown as mean ± SD. ****$P < 0.0001$.

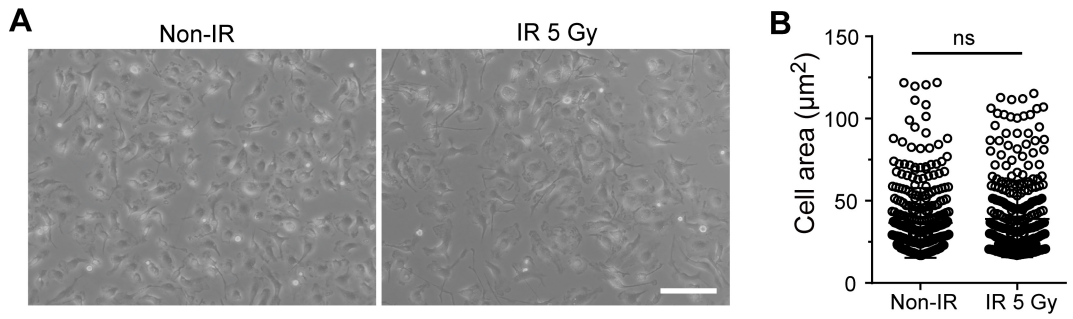

Figure S9. The morphology of BMDMs after irradiation. (A) Phase-contrast micrographs of BMDMs on the third day after 5 Gy irradiation. Scale bar, 100 μm. **(B)** Analysis of the cell area of (n = 123, 118 cells from three separate experiments, *t*-test). Values represent mean ± SD, ns, not significant.

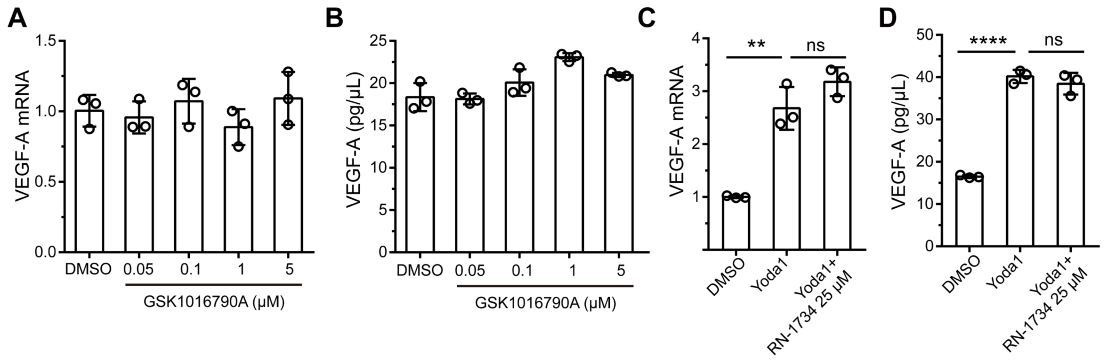

Figure S10. The role of TRPV4 in the expression of VEGF-A in BMDMs. (A) RT-PCR analysis of VEGF-A mRNA levels in BMDMs at 6 h after TRPV4 agonist GSK1016790A treatment **(B)** ELISA analysis of VEGF-A expression in BMDMs at 24 h after TRPV4 agonist GSK1016790A treatment. **(C)** RT-PCR analysis of VEGF-A mRNA levels in BMDMs pretreated with TRPV4 inhibitor RN-1734 for 30 min before 6 h Yoda1 (5 μM) treatment **(D)** ELISA analysis of VEGF-A expression in BMDMs pretreated with TRPV4 inhibitor RN-1734 for 30 min before 24 h Yoda1 (5 μM) treatment. n = 3 independent experiments, Tukey test. Data were shown as mean ± SD. $^{**}P < 0.01$; $^{****}P < 0.0001$; ns, not significant.